

An application of the tensor virial theorem to hole + vortex + bulge systems

R. Caimmi*

October 28, 2018

Abstract

The tensor virial theorem for subsystems is formulated for three-component systems and further effort is devoted to a special case where the inner subsystems and the central region of the outer one are homogeneous, the last surrounded by an isothermal homeoid. The virial equations are explicitly written under the additional restrictions: (i) similar and similarly placed inner subsystems, and (ii) spherical outer subsystem. An application is made to hole + vortex + bulge systems, in the limit of flattened inner subsystems, which implies three virial equations in three unknowns. Using the Faber-Jackson relation, $R_e \propto \sigma_0^2$, the standard M_H - σ_0 form ($M_H \propto \sigma_0^4$) is deduced from qualitative considerations. The projected bulge velocity dispersion to projected vortex velocity ratio, $\eta = (\sigma_B)_{33} / \{[(v_V)_{qq}]^2 + [(\sigma_V)_{qq}]^2\}^{1/2}$, as a function of the fractional radius, $y_{BV} = R_B/R_V$, and the fractional masses, $m_{BH} = M_B/M_H$ and $m_{BV} = M_B/M_V$, is studied in the range of interest, $0 \leq m_{VH} = M_V/M_H \leq 5$ (Escala, 2006) and $229 \leq m_{BH} \leq 795$ (Marconi and Hunt, 2003), consistent with observations. The related curves appear to be similar to Maxwell velocity distributions, which implies a fixed value of η below the maximum corresponds to two different configurations: a compact bulge on the left of the maximum, and an extended bulge on the right. All curves lie very close one to the other on the left of the maximum, and parallel

* *Astronomy Department, Padua Univ., Vicolo Osservatorio 2, I-35122 Padova, Italy*
email: roberto.caimmi@unipd.it

one to the other on the right. On the other hand, fixed m_{BH} or m_{BV} , and y_{BV} , are found to imply more massive bulges passing from bottom to top along a vertical line on the ($\text{O}y_{\text{BV}}\eta$) plane, and vice versa. The model is applied to NGC 4374 and NGC 4486, taking the fractional mass, m_{BH} , and the fractional radius, y_{BV} , as unknowns, and the bulge mass is inferred and compared with results from different methods. In presence of a massive vortex ($m_{\text{VH}} = 5$), the hole mass has to be reduced by a factor 2-3 with respect to the case of a massless vortex, to get the fit. Finally, the assumptions of homogeneous inner bulge and isotropic stress tensor are discussed.

keywords - *Black hole physics; galaxies: bulges. PACS codes* - 98.62.Js

1 Introduction

The existence of large masses confined in a restricted central region of galaxies (hereafter quoted as “holes”), is widely supported by current high-resolution observations (for a review see e.g., Ferrarese and Ford, 2005; Merritt, 2006). There is an amount of increasing evidence, that compact objects at the centre of (sufficiently large) galaxies are supermassive black holes (e.g., Maoz, 1998; Miller, 2006). In addition, the presence of self-gravitating nuclear disks (with typically several hundreds parsecs in radius; hereafter quoted as “outer vortexes”) seems necessary to continuously replenish inner Keplerian accretion disks (hereafter quoted as “inner vortexes”), allowing substantial hole mass growth (e.g., Escala, 2006). Hole growth can successfully be modelled as a rapid succession of vortexes with comparable mass, related to a merger event (King et al., 2008). Most of the gas residing in the outer, self-gravitating disk, is expected to be either turned into stars, or expelled by the first generation of high-luminosity stars, on a rapid (almost dynamical) time-scale (King et al., 2008).

In the following, the disk made of the inner vortex and the outer (self-gravitating) vortex, shall be quoted as the “vortex”. Masses up to about one fifth the inner bulge (i.e. bulge stars inside the isophote with equatorial axes coinciding with the edge of the vortex) have been deduced from observations (e.g., Downes and Solomon, 1998). The occurrence of vortexes is expected to be a common feature during the evolution of galaxies hosting holes. Accordingly, central regions of large galaxies may be modelled as the superposition of three main components: a central hole, a surrounding vortex, and an embedding bulge.

In this view, the tensor virial theorem for subsystems (Brosche et al., 1983; Caimmi et al., 1984; Caimmi and Secco, 1992; Caimmi, 2007) could

be a useful tool of investigation. In the case under discussion there are nine virial equations, three for each subsystem. In absence of a satisfactory theory of quantum gravity, the mass distribution within the hole cannot be described, which reduces the number of virial equations from nine to six. The further restriction to an axisymmetric gravitational potential, implying an axisymmetric matter distribution for each subsystem, further reduces the number of virial equations from six to four. The final restriction to flattened vortex and hole configurations, reduces the number of virial equations from four to three.

Keeping in mind that the virial theorem deals with global instead of local properties of matter distributions, simple even if unrealistic density profiles can be used for investigating main features and general trends. To this aim, the hole and the vortex are modelled as concentric and coaxial, flattened, homogeneous spheroids, the inner bulge as a homogeneous sphere, and the outer bulge as an isothermal spherical corona, which allows an analytical formulation (Caimmi and Secco, 2002).

To close the system of three equations, the number of unknowns must be reduced to three. The variables are: three mass-averaged square velocities, three masses, and three equatorial semiaxes. Hole mass and equatorial semi-axis can be related via the expression of the gravitational (or Schwarzschild) radius (e.g., Landau and Lifchitz, 1966, Chap. XI, §97). Typical values of bulge and vortex equatorial semiaxes, can be deduced from observations (e.g., Downes and Solomon, 1998). The vortex to hole mass ratio cannot exceed a value of about 5 (e.g., Escala, 2006), deduced from observations (Downes and Solomon, 1998). An empirical correlation seems to exist between bulge and hole mass (e.g., Marconi and Hunt, 2003). Mass-averaged bulge square velocities may safely be approximated by square luminosity-weighted second moments of the line-of-sight velocity distribution within the half-light radius, which is weakly dependent on the details of the orbital distribution (Capellari et al., 2006). In fact, a similar quantity is also used for studying the correlation between hole mass and bulge velocity dispersion (e.g., Gebhardt et al., 2000). Taking the above informations into due account, the number of unknowns in the virial equations may be reduced from nine to three.

In addition, the combination of two virial equations yields a relation between mass-averaged velocity ratios, mass ratios, and equatorial axis ratios, regardless of the values of mass-averaged velocities, masses, and equatorial semiaxes. For assigned bulge to vortex and vortex to hole mass ratios, and vortex to hole equatorial axis ratio, the mass-averaged bulge to vortex velocity ratio is a function of the bulge to vortex equatorial axis ratio, and the related trend can be studied. In particular, the bulge mass can be determined by the knowledge of other parameters, and the related value can be

compared with results from different methods.

The current paper is organized as follows. The virial theorem for subsystems, with regard to three-component systems, is formulated in Sect. 2. The model and its application to hole + vortex + bulge systems are the subject of Sect. 3, where the results are also presented and discussed, with regard to the special cases of NGC 4374 (M84) and NGC 4486 (M87). The conclusion is drawn in Sect. 4.

2 Basic theory

A general theory of two-component matter distributions has been exhaustively treated in earlier papers (e.g., Caimmi and Secco, 1992; Caimmi and Marmo, 2003; Caimmi and Valentinuzzi, 2008) and an interested reader is addressed therein and in parent investigations (MacMillan, 1930, Chap. III, §76; Limber, 1959; Neutsch, 1979; Brosche et al., 1983; Caimmi et al., 1984). The related tensor virial theorem is expressed by 3×2 independent equations, each containing $2 + (2 - 1)$ terms corresponding to the kinetic energy and the self potential energy of the subsystem under consideration, and to the tidal potential energy due to the gravitational potential induced by the other subsystem, respectively.

In dealing with N subsystems, the tensor virial theorem is expressed by $3 \times N$ independent equations, each containing $2 + (N - 1)$ terms corresponding to the kinetic energy and the self potential energy of the subsystem under consideration, and to the tidal potential energies due to the gravitational potential induced by the other subsystems, respectively. Accordingly, the results found for two-component systems can be used, by inserting in the virial equations $N - 2$ additional terms, related to the tidal potential energies of the extra components.

To this aim, the formulation of earlier attempts (Caimmi and Secco, 1992, 2002) shall be used. If not otherwise stated, for sake of convenience, matter distributions shall be conceived as continuous media instead of discrete particle sets (e.g., Limber, 1959; Caimmi, 2007). In the following, general definitions and related explicit expressions will be presented. Readers mainly interested to an application of astrophysical interest (hole + vortex + bulge systems) might directly go to the next Section 3.

2.1 The tensor virial theorem for subsystems

Let i, j, k , denote the subsystems of a three-component matter distribution. Owing to the additivity of the gravitational potential, the potential-energy

tensor and the potential energy may be cast into the form:

$$(E_{\text{pot}})_{pq} = \sum_u [(E_u)_{\text{sel}}]_{pq} + \sum_u \sum_v (1 - \delta_{uv}) [(E_{uv})_{\text{int}}]_{pq} \quad ; \quad (1a)$$

$$E_{\text{pot}} = \sum_u (E_u)_{\text{sel}} + \sum_u \sum_v (1 - \delta_{uv}) (E_{uv})_{\text{int}} \quad ; \quad (1b)$$

$$p = 1, 2, 3 \quad ; \quad q = 1, 2, 3 \quad ; \quad u = i, j, k \quad ; \quad uv = ij, ik, jk, ji, ki, kj \quad ; \quad (1c)$$

where δ_{uv} is the Kronecker symbol, $[(E_u)_{\text{sel}}]_{pq}$ and $(E_u)_{\text{sel}}$ the self potential-energy tensor and the self potential energy, respectively, $[(E_{uv})_{\text{int}}]_{pq}$ and $(E_{uv})_{\text{int}}$ the interaction potential-energy tensor and the interaction potential energy, respectively. The related explicit expressions are (e.g., Caimmi and Secco, 1992):

$$\begin{aligned} [(E_u)_{\text{sel}}]_{pq} &= \int_{S_u} \rho_u(x_1, x_2, x_3) x_p \frac{\partial \mathcal{V}_u}{\partial x_q} d^3 S_u \\ &= -\frac{1}{2} \int_{S_u} \rho_u(x_1, x_2, x_3) [\mathcal{V}_u(x_1, x_2, x_3)]_{pq} d^3 S_u \quad ; \end{aligned} \quad (2a)$$

$$\begin{aligned} (E_u)_{\text{sel}} &= \int_{S_u} \rho_u(x_1, x_2, x_3) \sum_{s=1}^3 x_s \frac{\partial \mathcal{V}_u}{\partial x_s} d^3 S_u \\ &= -\frac{1}{2} \int_{S_u} \rho_u(x_1, x_2, x_3) \mathcal{V}_u(x_1, x_2, x_3) d^3 S_u \quad ; \end{aligned} \quad (2b)$$

$$[(E_{uv})_{\text{int}}]_{pq} = -\frac{1}{2} \int_{S_u} \rho_u(x_1, x_2, x_3) [\mathcal{V}_v(x_1, x_2, x_3)]_{pq} d^3 S_u \quad ; \quad (3a)$$

$$(E_{uv})_{\text{int}} = -\frac{1}{2} \int_{S_u} \rho_u(x_1, x_2, x_3) \mathcal{V}_v(x_1, x_2, x_3) d^3 S_u \quad ; \quad (3b)$$

where S is the volume, ρ the density, \mathcal{V}_{pq} and \mathcal{V} the gravitational tensor potential and potential, respectively (Chandrasekhar, 1969, Chap. 2, §10).

The tensor and the scalar virial theorem for a single subsystem within the tidal field induced by the other ones, read:

$$2[(E_u)_{\text{kin}}]_{pq} + [(E_u)_{\text{sel}}]_{pq} + [(E_{uv})_{\text{tid}}]_{pq} + [(E_{uv})_{\text{tid}}]_{pq} = 0 \quad ; \quad (4a)$$

$$2(E_u)_{\text{kin}} + (E_u)_{\text{sel}} + (E_{uv})_{\text{tid}} + (E_{uv})_{\text{tid}} = 0 \quad ; \quad (4b)$$

$$u = i, j, k \quad ; \quad v = j, k, i \quad ; \quad w = k, i, j \quad ; \quad (4c)$$

where $[(E_u)_{\text{kin}}]_{pq}$ and $(E_u)_{\text{kin}}$ are the kinetic-energy tensor and the kinetic energy, respectively, $[(E_{uv})_{\text{tid}}]_{pq}$ and $(E_{uv})_{\text{tid}}$ the tidal potential-energy tensor and the tidal potential energy, respectively. The related explicit expressions

are (e.g., Caimmi and Valentinuzzi, 2008):

$$[(E_u)_{\text{kin}}]_{pq} = \frac{1}{2} \int_{S_u} \rho_u(x_1, x_2, x_3) (v_u)_p (v_u)_q d^3 S_u ; \quad (5a)$$

$$(E_u)_{\text{kin}} = \frac{1}{2} \int_{S_u} \rho_u(x_1, x_2, x_3) \sum_{s=1}^3 [(v_u)_s]^2 d^3 S_u ; \quad (5b)$$

$$[(E_{uv})_{\text{tid}}]_{pq} = \int_{S_u} \rho_u(x_1, x_2, x_3) x_p \frac{\partial \mathcal{V}_v}{\partial x_q} d^3 S_u ; \quad (6a)$$

$$(E_{uv})_{\text{tid}} = \int_{S_u} \rho_u(x_1, x_2, x_3) \sum_{s=1}^3 x_s \frac{\partial \mathcal{V}_v}{\partial x_s} d^3 S_u ; \quad (6b)$$

where $(v_u)_p (v_u)_q = \overline{(v_u)_p (v_u)_q}$ and $[(v_u)_s]^2 = \overline{[(v_u)_s]^2}$ are arithmetic means calculated within the infinitesimal volume element, $d^3 S_u = dx_1 dx_2 dx_3$, placed at $\mathbf{P}(x_1, x_2, x_3)$ (Binney and Tremaine, 1987, Chap. 4, §4.3). The tidal potential energy may be conceived as the virial of the u component in connection with the tidal field induced by the v component (Brosche et al., 1983).

The tensor and the scalar virial theorem, expressed by Eqs. (4a) and (4b), are the extension of earlier results related to one-component (e.g., Chandrasekhar, 1969, Chap. II, §11; Binney and Tremaine, 1987, Chap. 4, §3) and two-component (e.g., Caimmi et al., 1984; Caimmi and Secco, 1992) systems.

The tensor and the scalar virial theorem for the whole system read:

$$2(E_{\text{kin}})_{pq} + (E_{\text{pot}})_{pq} = 0 ; \quad (7a)$$

$$2E_{\text{kin}} + E_{\text{pot}} = 0 ; \quad (7b)$$

which can be made explicit using Eqs. (1a)-(1b). An alternative formulation can be obtained summing Eqs. (4a)-(4b) over all the subsystems. The combination of the related expressions yields:

$$[(E_{uv})_{\text{tid}}]_{pq} + [(E_{vu})_{\text{tid}}]_{pq} = [(E_{uv})_{\text{int}}]_{pq} + [(E_{vu})_{\text{int}}]_{pq} ; \quad (8a)$$

$$(E_{uv})_{\text{tid}} + (E_{vu})_{\text{tid}} = (E_{uv})_{\text{int}} + (E_{vu})_{\text{int}} ; \quad (8b)$$

$$uv = ij, ik, jk ; \quad vu = ji, ki, kj ; \quad (8c)$$

according to earlier results related to two-component systems (Caimmi and Secco, 1992).

In the general case of subsystems with different shapes, the tensor and scalar virial equations, Eqs. (4a) and (4b), need numerical integrations to be made explicit, except for concentric and coaxial homogeneous ellipsoids, one completely lying within the other (e.g., Caimmi and Secco, 1992). The effect of different shapes is larger for flat density profiles, with respect to their

monotonically decreasing counterparts. Explicit formulae also exist if the outer ellipsoid, in turn, is surrounded by a similar and similarly placed heterogeneous homeoid, where the inner surface coincides with the boundary of the outer ellipsoid (Caimmi and Secco, 2002). In the more realistic situation of homeoidally striated ellipsoids (Roberts, 1962), a further restriction aimed to simplify the calculations, is that different subsystems are also similar and similarly placed (e.g., Caimmi, 1993; Caimmi and Marmo, 2003; Caimmi and Valentinuzzi, 2008).

In dealing with an application of the tensor virial theorem to a three-component system of astrophysical interest, the choice of the related density profiles shall be limited to the above mentioned special cases.

3 The model

3.1 The hole, the vortex, and the bulge

Aiming to a simple application of the tensor virial theorem, inner regions of large galaxies shall be idealized as three-component systems, one completely lying within the other: the hole, the vortex, and the bulge, respectively. The outer vortex is self-gravitating, and the presence of the inner vortex allows mass accretion inside the last stable orbit. The inner bulge is enclosed by the isopycnic (i.e. constant density) surface with equatorial axes coinciding with the edge of the vortex.

In absence of a satisfactory theory of quantum gravity, the mass distribution within the hole cannot be described, which reduces the number of tensor virial equations, Eqs. (4a), from nine to six. The further restriction to an axisymmetric gravitational potential, implying an axisymmetric density profile, for each subsystem, further reduces the number of tensor virial equations from six to four. The final restriction to flattened vortex configurations, reduces the number of tensor virial equations from four to three.

The hole shall be modelled by a flattened homogeneous spheroid potential, where the equatorial axis coincides with the radius of the particle inner stable circular orbit of the related Schwarzschild black hole:

$$R_{\text{H}} = 3R_g \ ; \quad R_g = \frac{2GM_{\text{H}}}{c^2} \ ; \quad (9)$$

where G is the constant of gravitation, c is the light velocity in (baryonic) vacuum, M is the mass, R_g is the gravitational radius (e.g., Landau and Lifchitz, 1966, Chap. XI, §97), and the index, H, denotes the hole. The choice of a Plummer potential (Escala, 2006) would imply a more complicated formulation (Caimmi and Valentinuzzi, 2008). The selected value for R_{H} , expressed

by Eq.(9) and related to Schwarzschild's metrics, makes an acceptable compromise between a corotating particle inner stable circular orbit radius, $R_{\text{H}} = (1/2)R_g$, and its counterrotating counterpart, $R_{\text{H}} = (9/2)R_g$, related to Kerr's metrics. For the photon inner stable circular orbit, $R_{\text{H}} = (3/2)R_g$ in Schwarzschild's metrics, and $R_{\text{H}} = (1/2)R_g$ (corotating), $R_{\text{H}} = 2R_g$ (counterrotating), in Kerr's metrics. For further details refer to specialized reviews (e.g., Bilic, 2006).

The vortex may be conceived, to a first extent, as self-gravitating even if it is still not clear if fragmentation or turbulence are dominating (e.g., Escala, 2006). For simplicity, both the vortex circular velocity, v , and the inner bulge velocity dispersion, σ , are assumed constant with radius, which is only strictly valid for an isothermal sphere (Escala, 2006). Even within the most massive gaseous vortexes known so far, the gravitational potential is dominated by the inner bulge. With regard to the inner bulge, the following values are deduced from observations (Downes and Solomon, 1998):

$$m_{\text{IN}} = \frac{M_{\text{I}}}{M_{\text{V}}} \approx 5 \quad ; \quad (10)$$

where M_{V} and M_{I} are the mass of the gaseous vortex and stellar inner bulge, respectively.

The circular velocity at the edge of the vortex, is obtained by the condition of centrifugal equilibrium, as:

$$(v_{\text{V}})^2 = \frac{\zeta_{\text{V}}}{m_{\text{IN}}} \frac{GM_{\text{I}}}{R_{\text{V}}} + \frac{\zeta_{\text{H}}}{m_{\text{IH}}} \frac{GM_{\text{I}}}{R_{\text{V}}} + \zeta_{\text{I}} \frac{GM_{\text{I}}}{R_{\text{V}}} \quad ; \quad (11)$$

where ζ is a shape factor and, in particular, $\zeta = 1$ for spherical-symmetric mass distributions and $\zeta = \pi/2$ for flattened homogeneous spheroids.

The inner bulge velocity dispersion at the edge of the vortex reads:

$$(\sigma_{\text{I}})^2 = \frac{GM_{\text{I}}}{R_{\text{V}}} \quad ; \quad (12)$$

provided the density profile declines as in an isothermal sphere.

The combination of Eqs. (10)-(12) yields:

$$(v_{\text{V}})^2 = \left(\frac{\zeta_{\text{V}}}{m_{\text{IN}}} + \frac{\zeta_{\text{H}}}{m_{\text{IH}}} + \zeta_{\text{I}} \right) (\sigma_{\text{I}})^2 \approx (\sigma_{\text{I}})^2 \quad ; \quad (13)$$

which holds *a fortiori* for less massive vortexes, $m_{\text{IN}} > 5$.

The validity of the vortex steady state model (the so called α disk) as a zeroth order approximation, has successfully been tested by recent numerical

experiments (Escala, 2006). The vortex shall be represented as a flattened homogeneous spheroid potential, similar and similarly placed with respect to the hole.

Strictly speaking, the mass inside the hole volume should be subtracted which, in the case under discussion, amounts to:

$$\Delta M_V = \left(\frac{R_H}{R_V} \right)^3 M_V ; \quad (14)$$

and the ratio of subtracted to remaining mass reads:

$$\frac{\Delta M_V}{M_V - \Delta M_V} = \frac{(R_H/R_V)^3}{1 - (R_H/R_V)^3} ; \quad (15)$$

which shows that the subtracted mass, ΔM_V , may safely be neglected.

The inner bulge, $0 \leq r \leq R_V$, shall be modelled by a homogeneous sphere potential, and similar considerations can be made for the subtracted mass:

$$\Delta M_I = \left(\frac{R_H}{R_I} \right)^3 M_I ; \quad (16)$$

keeping in mind that $R_I = R_V$.

The outer bulge, $R_V \leq r \leq R_B$, shall be modelled by a truncated isothermal sphere potential. The related density profile (including the inner bulge) is:

$$\rho_B = \rho_V f_B(\xi_B) ; \quad \xi_B = \frac{r}{R_B} ; \quad (y_{BV})^{-1} = \frac{R_V}{R_B} ; \quad (17a)$$

$$f_B(\xi_B) = \begin{cases} 1 ; & 0 \leq \xi_B \leq (y_{BV})^{-1} ; \\ (y_{BV}\xi_B)^{-2} ; & (y_{BV})^{-1} \leq \xi_B \leq 1 ; \end{cases} \quad (17b)$$

where, in general, $r_{NB} = R_V$ and $\rho_{NB} = \rho_V$ are a scaling radius and a scaling density, respectively.

In conclusion, the central part of a large galaxy shall be modelled as an inner, flattened homogeneous spheroid (the hole), embedded within a similar and similarly placed, flattened homogeneous spheroid (the vortex) which, in turn, is lying within a homogeneous sphere with equal equatorial semiaxes (the inner bulge), surrounded by a concentric, isothermal, spherical corona (the outer bulge).

3.2 The tensor virial equations

The four tensor virial equations which, among the nine expressed by Eqs. (4), are relevant to the application of interest, are:

$$2[(E_V)_{\text{kin}}]_{\text{pp}} + [(E_V)_{\text{sel}}]_{\text{pp}} + [(E_{VH})_{\text{tid}}]_{\text{pp}} + [(E_{VB})_{\text{tid}}]_{\text{pp}} = 0 ; \quad (18a)$$

$$2[(E_B)_{\text{kin}}]_{\text{pp}} + [(E_B)_{\text{sel}}]_{\text{pp}} + [(E_{BH})_{\text{tid}}]_{\text{pp}} + [(E_{BV})_{\text{tid}}]_{\text{pp}} = 0 ; \quad (18b)$$

where x_3 has been chosen as symmetry axis, which implies $p = 1, 3$, and all the terms may be written explicitly, under the assumptions previously made.

The vortex and the bulge kinetic-energy tensors read:

$$2 [(E_V)_{\text{kin}}]_{pp} = M_V \left\{ (1 - \delta_{3p}) [(v_V)_{pp}]^2 + [(\sigma_V)_{pp}]^2 \right\} ; \quad (19a)$$

$$2 [(E_B)_{\text{kin}}]_{pp} = M_B \left\{ (1 - \delta_{3p}) [(v_B)_{pp}]^2 + [(\sigma_B)_{pp}]^2 \right\} ; \quad (19b)$$

$$v_V \approx \sigma_B ; \quad p = 1, 3 ; \quad (19c)$$

where δ is the Kronecker symbol, v_{pp} and σ_{pp} are the circular velocity and the random velocity components along the corresponding axis, respectively.

In the special case of homeoidally striated ellipsoids (Roberts, 1962), the self-potential energy tensors read (e.g., Caimmi, 1993):

$$[(E_X)_{\text{sel}}]_{pp} = -(\nu_X)_{\text{sel}} \frac{GM_X^2}{R_X} (B_X)_p ; \quad X = V, B ; \quad (20a)$$

$$B_p = \epsilon_{p2}\epsilon_{p3} \int_0^{+\infty} (1+s)^{-3/2} (1+\epsilon_{p\ell}^2 s)^{-1/2} (1+\epsilon_{pr}^2 s)^{-1/2} ds ; \quad (20b)$$

$$\epsilon_{pq} = \frac{a_p}{a_q} ; \quad p = 1, 2, 3 ; \quad q = 1, 2, 3 ; \quad p \neq \ell \neq r ; \quad (20c)$$

where R is the major equatorial semiaxis, $(\nu_X)_{\text{sel}}$ are profile factors, B_p shape factors which, for axisymmetric configurations, may be analytically expressed (e.g., Chandrasekhar, 1969, Chap. 3, §21; Caimmi, 1991, 1995), and ϵ_{pq} axis ratios. For further details refer to Appendix A.

The vortex self potential energy profile factor reads (Caimmi and Secco, 1992):

$$(\nu_V)_{\text{sel}} = \frac{3}{10} ; \quad (21)$$

and the shape factors are expressed in Appendix A.

The bulge self potential energy profile factor reads (Caimmi and Secco, 2002)¹:

$$(\nu_B)_{\text{sel}} = \frac{3}{10} \frac{15(y_{BV})^2 - 14y_{BV} - 10y_{BV} \ln(y_{BV})}{(3y_{BV} - 2)^2} ; \quad (22)$$

related to the density profile, expressed by Eq. (17).

In the general case of triaxial configurations, the tidal potential-energy tensors depend on the density profiles and on the shape of the ellipsoids. The isopycnic surface of the outer ellipsoid which is still embedding the inner

¹The related formula in the parent paper, Eq. (51) therein, is different due to printing errors.

one, is tangent to the latter boundary at a top axis, $(a_i)_t$. For oblate-like configurations, the inner more flattened than the outer, $(a_i)_t = (a_i)_1$.

The mass of the outer ellipsoid surrounded by the isothermal homeoid, is (Caimmi and Secco, 2002)²:

$$M_B = (\nu_B)_{\text{mas}} (M_B)_0 ; \quad (23a)$$

$$(M_B)_0 = \frac{4\pi}{3} (\rho_B)_0 (a_B)_1 (a_B)_2 (a_B)_3 ; \quad (23b)$$

$$(\nu_B)_{\text{mas}} = (y_{BV})^{-3} [1 + 3(y_{BV} - 1)] ; \quad (23c)$$

$$y_{BV} = (y_{BV})_t = \frac{(a_B)_t}{(a_V)_t} ; \quad (23d)$$

where $(\rho_B)_0$ is the central density, $(M_B)_0$ the mass of a homogeneous ellipsoid with same boundary and density equal to the central density, and the major axis of the inner bulge and the vortex coincide. Accordingly, Eq. (23a) takes the equivalent form:

$$M_B = M_I [1 + 3(y_{BV} - 1)] ; \quad (24)$$

where M_I is the mass of the inner bulge.

In the special case of two concentric and coaxial homogeneous ellipsoids, the more flattened one completely lying within the other with a tangential point at the top major equatorial semiaxis, R_X , surrounded by a isothermal (X=V) or homogeneous + isothermal (X=H) homeoid where the inner surface coincides with the boundary of the outer ellipsoid, the tidal potential-energy tensors read (Caimmi and Secco, 2001, 2002):

$$[(E_{XY})_{\text{tid}}]_{pq} = -\delta_{pq} \frac{GM_X^2}{R_X} (\nu_{XY})_{\text{tid}} \frac{[(y_{YX})_1]^2}{[(y_{YX})_p]^2} (B_Y)_p ; \quad (25a)$$

$$[(E_{YX})_{\text{tid}}]_{pq} = -\delta_{pq} \frac{GM_X^2}{R_X} (\nu_{XY})_{\text{tid}} \left\{ \frac{5}{2} [(y_{YX})_1]^2 F_Y(y_{YX}) + (\Phi_{YX})_p \right\} (B_Y)_p ; \quad (25b)$$

$$(\nu_{XY})_{\text{tid}} = \frac{3}{10} \frac{m_{YX}}{[(y_{YX})_1]^3} \frac{1}{(\nu_Y)_{\text{mas}}} ; \quad m_{YX} = \frac{M_Y}{M_X} ; \quad (y_{YX})_p = \frac{(a_Y)_p}{(a_X)_p} > 1 ; \quad (25c)$$

$$\frac{(\epsilon_X)_{pq}}{(\epsilon_Y)_{pq}} = \frac{(y_{YX})_q}{(y_{YX})_p} ; \quad X = H, V ; \quad Y = B ; \quad p = 1, 2, 3 ; \quad q = 1, 2, 3 ; \quad (25d)$$

$$F_B(y_{BV}) = 2 \frac{\ln(y_{BV})}{(y_{BV})^2} ; \quad F_B(y_{BH}) = \frac{1}{(y_{BV})^2} - \frac{1}{(y_{BH})^2} + 2 \frac{\ln(y_{BV})}{(y_{BV})^2} ; \quad (25e)$$

²With regard to the profile factor, the related formula in the parent paper, Eq. (49) therein, is different due to printing errors. In addition, ξ_k^2 has to be replaced by ξ_k^3 in Eq. (50) therein.

$$(\Phi_{\text{YX}})_p = \frac{5}{2} - \frac{3}{2} \left[\frac{(y_{\text{YX}})_1}{(y_{\text{YX}})_p} \right]^2 - \frac{1}{2} \sum_{r=1}^3 \left\{ \left[\frac{(y_{\text{YX}})_1}{(y_{\text{YX}})_r} \right]^2 - \left[\frac{(y_{\text{YX}})_1}{(y_{\text{YX}})_p} \right]^2 \right\} \frac{(B_{\text{Y}})_{pr}}{(B_{\text{Y}})_p} ; \quad (25\text{f})$$

$$B_{pr} = \epsilon_{p2}\epsilon_{p3} \int_0^{+\infty} (1+s)^{-3/2} (1+\epsilon_{p\ell}^2 s)^{-1/2} (1+\epsilon_{pr}^2 s)^{-3/2} ds ; \quad (25\text{g})$$

$$p = 1, 2, 3 ; \quad \ell = 1, 2, 3 ; \quad r = 1, 2, 3 ; \quad p \neq \ell \neq r ; \quad (25\text{h})$$

where ν_{tid} are profile factors and B_{pr} are shape factors which, for axisymmetric configurations, may be analytically expressed (e.g., Chandrasekhar, 1969, Chap. 3, §21; Caimmi, 1995). For further details refer to Appendix A.

In the special case of two concentric and coaxial homogeneous ellipsoids, one completely lying within the other (e.g., Caimmi and Secco, 1992), the tidal potential-energy tensors read:

$$[(E_{\text{HV}})_{\text{tid}}]_{pq} = -\delta_{pq} \frac{GM_{\text{H}}^2}{R_{\text{H}}} (\nu_{\text{HV}})_{\text{tid}} \frac{[(y_{\text{VH}})_1]^2}{[(y_{\text{VH}})_p]^2} (B_{\text{V}})_p ; \quad (26\text{a})$$

$$[(E_{\text{VH}})_{\text{tid}}]_{pq} = -\delta_{pq} \frac{GM_{\text{H}}^2}{R_{\text{H}}} (\nu_{\text{HV}})_{\text{tid}} [F_{\text{V}}(y_{\text{VH}}) + (\Phi_{\text{VH}})_p] (B_{\text{V}})_p ; \quad (26\text{b})$$

$$(\nu_{\text{HV}})_{\text{tid}} = \frac{3}{10} \frac{m_{\text{VH}}}{[(y_{\text{VH}})_1]^3} \frac{1}{(\nu_{\text{V}})_{\text{mas}}} ; \quad (\nu_{\text{H}})_{\text{mas}} = (\nu_{\text{V}})_{\text{mas}} = 1 ; \quad (26\text{c})$$

$$F_{\text{V}}(y_{\text{VH}}) = \frac{5}{2} \left[\frac{(y_{\text{VH}})_1}{(y_{\text{VH}})_p} \right]^2 \left\{ [(y_{\text{VH}})_p]^2 - \left[\frac{(y_{\text{VH}})_p}{(y_{\text{VH}})_t} \right]^2 \right\} ; \quad (26\text{d})$$

which may be conceived as a three-component system, as discussed above, where the surrounding homeoid is homogeneous instead of isothermal or homogeneous + isothermal.

In the special case under discussion, the shape factors take the expression:

$$(\Phi_{\text{YX}})_1 = (\Phi_{\text{YX}})_2 = 1 + \frac{3}{10}(1 - \epsilon^2) ; \quad (27\text{a})$$

$$(\Phi_{\text{YX}})_3 = 1 + \frac{9}{10}(1 - \epsilon^2) ; \quad (27\text{b})$$

$$(\Phi_{\text{VH}})_1 = (\Phi_{\text{VH}})_2 = (\Phi_{\text{VH}})_3 = 1 ; \quad (27\text{c})$$

$$\epsilon_{\text{H}} = \epsilon_{\text{V}} = \epsilon ; \quad \epsilon_{\text{B}} = 1 ; \quad (27\text{d})$$

$$\frac{(a_{\text{V}})_p}{(a_{\text{V}})_r} = \frac{(a_{\text{H}})_p}{(a_{\text{H}})_r} ; \quad (y_{\text{VH}})_p = (y_{\text{VH}})_r = y_{\text{VH}} ; \quad (27\text{e})$$

and the four tensor virial equations of interest, Eqs. (18), due to (19)-(27), may be written under the explicit form:

$$[(v_{\text{V}})_{qq}]^2 + [(\sigma_{\text{V}})_{qq}]^2 = \frac{3}{10} \frac{GM_{\text{V}}}{R_{\text{V}}} \left\{ \frac{\alpha}{\epsilon} \left[1 + \frac{1}{m_{\text{VH}}(y_{\text{VH}})^2} \left(\frac{5}{2}(y_{\text{VH}})^2 - \frac{3}{2} \right) \right] \right\}$$

$$+ \frac{2}{3} \frac{m_{\text{BV}}}{3y_{\text{BV}} - 2} \left[\frac{(y_{\text{BV}})_1}{(y_{\text{BV}})_q} \right]^2 \left[\frac{(y_{\text{BV}})_t}{(y_{\text{BV}})_1} \right]^3 \Big\} ; \quad q = 1, 2 ; \quad (28a)$$

$$[(\sigma_{\text{V}})_{33}]^2 = \frac{3}{10} \frac{GM_{\text{V}}}{R_{\text{V}}} \left\{ \epsilon\gamma \left[1 + \frac{1}{m_{\text{VH}}(y_{\text{VH}})^2} \left(\frac{5}{2}(y_{\text{VH}})^2 - \frac{3}{2} \right) \right] \right. \\ \left. + \frac{2}{3} \frac{m_{\text{BV}}}{3(y_{\text{BV}})_t - 2} \left[\frac{(y_{\text{BV}})_1}{(y_{\text{BV}})_3} \right]^2 \left[\frac{(y_{\text{BV}})_t}{(y_{\text{BV}})_1} \right]^3 \right\} ; \quad (28b)$$

$$[(v_{\text{B}})_{qq}]^2 + [(\sigma_{\text{B}})_{qq}]^2 = \frac{1}{5} \frac{GM_{\text{B}}}{R_{\text{B}}} \left\{ \frac{15(y_{\text{BV}})^2 - 14y_{\text{BV}} - 10y_{\text{BV}} \ln(y_{\text{BV}})}{(3y_{\text{BV}} - 2)^2} \right. \\ \left. + \frac{1}{m_{\text{BH}}(y_{\text{VH}})^2} \left[\frac{(y_{\text{BH}})_t}{(y_{\text{BH}})_1} \right]^2 \frac{y_{\text{BV}}}{3y_{\text{BV}} - 2} \left\{ \frac{5}{2} \left[\frac{(y_{\text{BH}})_1}{(y_{\text{BH}})_t} \right]^2 \right. \right. \\ \left. \left. \times \left[(y_{\text{VH}})^2 - 1 + 2(y_{\text{VH}})^2 \ln(y_{\text{BV}}) \right] + 1 + \frac{3}{10} (1 - \epsilon^2) \right\} + \frac{1}{m_{\text{BV}}} \left[\frac{(y_{\text{BV}})_t}{(y_{\text{BV}})_1} \right]^2 \right. \\ \left. \times \frac{y_{\text{BV}}}{3y_{\text{BV}} - 2} \left[5 \left[\frac{(y_{\text{BV}})_1}{(y_{\text{BV}})_t} \right]^2 \ln(y_{\text{BV}}) + 1 + \frac{3}{10} (1 - \epsilon^2) \right] \right\} ; \quad q = 1, 2 ; \quad (28c)$$

$$[(\sigma_{\text{B}})_{33}]^2 = \frac{1}{5} \frac{GM_{\text{B}}}{R_{\text{B}}} \left\{ \frac{15(y_{\text{BV}})^2 - 14y_{\text{BV}} - 10y_{\text{BV}} \ln(y_{\text{BV}})}{(3y_{\text{BV}} - 2)^2} \right. \\ \left. + \frac{1}{m_{\text{BH}}(y_{\text{VH}})^2} \left[\frac{(y_{\text{BH}})_t}{(y_{\text{BH}})_1} \right]^2 \frac{y_{\text{BV}}}{3y_{\text{BV}} - 2} \left\{ \frac{5}{2} \left[\frac{(y_{\text{BH}})_1}{(y_{\text{BH}})_t} \right]^2 \right. \right. \\ \left. \left. \times \left[(y_{\text{VH}})^2 - 1 + 2(y_{\text{VH}})^2 \ln(y_{\text{BV}}) \right] + 1 + \frac{9}{10} (1 - \epsilon^2) \right\} + \frac{1}{m_{\text{BV}}} \left[\frac{(y_{\text{BV}})_t}{(y_{\text{BV}})_1} \right]^2 \right. \\ \left. \times \frac{y_{\text{BV}}}{3y_{\text{BV}} - 2} \left[5 \left[\frac{(y_{\text{BV}})_1}{(y_{\text{BV}})_t} \right]^2 \ln(y_{\text{BV}}) + 1 + \frac{9}{10} (1 - \epsilon^2) \right] \right\} ; \quad (28d)$$

where, in the special case of flattened configurations, $\epsilon = 0$, the shape factors reduce to $\alpha/\epsilon = \pi/2$ and $\epsilon\gamma = 0$, see Appendix A, which yields $(\sigma_{\text{V}})_{33} = 0$, as expected. The validity of Eqs. (28c) and (28d) implies an anisotropic bulge stress tensor, $[(v_{\text{B}})_{qq}]^2 + [(\sigma_{\text{B}})_{qq}]^2 < [(\sigma_{\text{B}})_{33}]^2$, which is due to the presence of more flattened, inner subsystems. In fact, an anisotropic stress tensor is necessary to maintain a spherical shape in the case under discussion.

The tensor virial equations, Eqs. (28a)-(28d), make a system of four equations in thirteen unknowns: two rotation velocity components, $(v_{\text{V}})_{11} = (v_{\text{V}})_{22}$ and $(v_{\text{B}})_{11} = (v_{\text{B}})_{22}$; four peculiar velocity components, $(\sigma_{\text{V}})_{11} = (\sigma_{\text{V}})_{22}$, $(\sigma_{\text{V}})_{33}$, $(\sigma_{\text{B}})_{11} = (\sigma_{\text{B}})_{22}$, and $(\sigma_{\text{B}})_{33}$; three masses, M_{H} , M_{V} , and M_{B} ; three major equatorial semiaxes, R_{H} , R_{V} , and R_{B} ; and one axis ratio, $\epsilon = \epsilon_{\text{H}} = \epsilon_{\text{V}}$. The hole mass, M_{H} , and the model hole major semiaxis, R_{H} ,

are connected via Eq. (9), which reduces the number of unknowns to twelve. Further reduction can be made using observational constraints and/or additional assumptions.

Rotation and peculiar velocity components could be deduced from observations, together with the vortex and bulge major semiaxes. The remaining four unknowns would be three masses and one axis ratio. In the flat limit ($\epsilon \rightarrow 0$) Eq. (28b) reduces to an indeterminate form, $0 = 0$, leaving three equations in three unknowns, M_H , M_V , and M_B . Of course, any other alternative might be exploited, yielding a system of four (or three) equations in four (or three) unknowns.

3.3 Application

According to an earlier model of massive vortexes (Escala, 2006), the hole and the vortex mass shall be taken as $M_H = 10^7 m_\odot$ and $M_V = 5 \cdot 10^7 m_\odot$, respectively. A flat disk ($\epsilon_H = \epsilon_V = 0$) makes an acceptable approximation to an assumed major equatorial semiaxis, $R_V = 125 \text{pc}$, and thickness, $Z_V = 4 \text{pc}$, (Escala, 2006) implying $\epsilon_V = Z_V/R_V = 0.032$. The particularization of Eq. (9) to the selected hole mass yields: $R_H = 2.87 \cdot 10^{-6} \text{pc}$.

The related parameters appearing in Eqs. (28a)-(28d) are:

$$m_{\text{VH}} = 5 \quad ; \quad y_{\text{VH}} = 4.35 \cdot 10^7 \quad ; \quad \epsilon = 0 \quad ; \quad (29)$$

and the substitution into the above mentioned equations, keeping in mind that Eq. (28b) cannot be used for flat configurations, yields:

$$[(v_V)_{qq}]^2 + [(\sigma_V)_{qq}]^2 = \frac{1}{5} \frac{GM_V}{R_V} \left\{ \frac{3\pi}{4} \left(1 + \frac{5}{2} \frac{1}{m_{\text{VH}}} \right) + \frac{m_{\text{BV}}}{3y_{\text{BV}} - 2} \right\} \quad ; \quad (30a)$$

$$\begin{aligned} [(v_B)_{qq}]^2 + [(\sigma_B)_{qq}]^2 &= \frac{1}{5} \frac{GM_B}{R_B} \left\{ \frac{15(y_{\text{BV}})^2 - 14y_{\text{BV}} - 10y_{\text{BV}} \ln(y_{\text{BV}})}{(3y_{\text{BV}} - 2)^2} \right. \\ &+ \left. \frac{1}{m_{\text{BH}}} \frac{y_{\text{BV}}}{3y_{\text{BV}} - 2} \frac{5}{2} [1 + 2 \ln(y_{\text{BV}})] + \frac{1}{m_{\text{BV}}} \frac{y_{\text{BV}}}{3y_{\text{BV}} - 2} \left[5 \ln(y_{\text{BV}}) + \frac{13}{10} \right] \right\} \quad ; \end{aligned} \quad (30b)$$

$$\begin{aligned} [(\sigma_B)_{33}]^2 &= \frac{1}{5} \frac{GM_B}{R_B} \left\{ \frac{15(y_{\text{BV}})^2 - 14y_{\text{BV}} - 10y_{\text{BV}} \ln(y_{\text{BV}})}{(3y_{\text{BV}} - 2)^2} \right. \\ &+ \left. \frac{1}{m_{\text{BH}}} \frac{y_{\text{BV}}}{3y_{\text{BV}} - 2} \frac{5}{2} [1 + 2 \ln(y_{\text{BV}})] + \frac{1}{m_{\text{BV}}} \frac{y_{\text{BV}}}{3y_{\text{BV}} - 2} \left[5 \ln(y_{\text{BV}}) + \frac{19}{10} \right] \right\} \quad ; \end{aligned} \quad (30c)$$

where the terms containing negative powers of $y_{\text{VH}} \gg 1$ and $y_{\text{BH}} > y_{\text{VH}}$, have been neglected.

In the current model, the vortex is described as a homogeneous, self-gravitating, flattened spheroid, which implies the relations:

$$\frac{1}{2}I_V\Omega_V^2 = \frac{1}{2}M_V\overline{[(v_V)^2]} = 2\frac{(E_V)_{\text{kin}}}{M_V} ; \quad (\sigma_V)_{qq} \ll (v_V)_{qq} ; \quad (31a)$$

$$I_V\Omega_V^2 = \frac{2}{5}M_V(R_V)^2\Omega_V^2 = \frac{2}{5}M_V[v_V(R_V)]^2 ; \quad (31b)$$

where Ω_V is the (solid-body) angular velocity, $\overline{[(v_V)^2]}$ the mean square rotation velocity, and $v_V(R_V) = \{2.5\overline{[(v_V)^2]}\}^{1/2}$ the rotation velocity at the edge. Strictly speaking, the presence of the hole implies differential rotation towards Keplerian velocities, but this effect can be neglected beyond the hole sphere of influence (e.g., Ferrarese and Ford, 2005). For the selected reference case, Eqs. (30) yield $[(v_V)_{qq}]^2/[(\sigma_V)_{33}]^2 \approx 0.4$ or $\{[v_V(R_V)]_{qq}\}^2/[(\sigma_V)_{33}]^2 \approx 1$, which is consistent with Eq. (13), as expected for massive inner bulges (e.g., Escala, 2006).

In the limit of null vortex and hole mass, Eq. (30c) reduces to:

$$[(\sigma_{B0})_{33}]^2 = \frac{1}{5} \frac{GM_B}{R_B} \frac{15(y_{BV})^2 - 14y_{BV} - 10y_{BV} \ln(y_{BV})}{(3y_{BV} - 2)^2} ; \quad (32)$$

and the combination of Eqs. (30c) and (32) yields:

$$\frac{1}{m_{BH}} = \frac{M_H}{M_B} = \frac{R_B [(\sigma_B)_{33}]^2}{GM_B} \left\{ 1 - \left[\frac{(\sigma_{B0})_{33}}{(\sigma_B)_{33}} \right]^2 \right\} \zeta(m_{BH}, y_{BV}) ; \quad (33a)$$

$$\zeta(m_{BH}, y_{BV}) = \frac{3y_{BV} - 2}{y_{BV}} \left[\frac{1}{2} + (1 + m_{VH}) \ln(y_{BV}) + \frac{19}{50}m_{VH} \right]^{-1} ; \quad (33b)$$

where in the range of interest, $1 \leq y_{BV} \leq 10^4$, $0 \leq m_{VH} \leq 5$, the contribution of the factor, $\zeta(m_{BH}, y_{BV})$, scales from about 0.05 to 2, related to $(m_{VH}, y_{BV}) = (5, 10^4)$, $(0, 1)$, respectively. A selected reference case, $(m_{VH}, y_{BV}) = (5, 14)$, yielding $M_B = 10^{10}m_\odot$ for an assumed $M_H = 10^7m_\odot$, corresponds to $\zeta(5, 14) = 0.156690$. In the limit of an infinitely extended bulge, $y_{BV} \rightarrow +\infty$, $\zeta(m_{BH}, y_{BV}) \rightarrow 0$, due to $M_B \rightarrow +\infty$, for the isothermal sphere. Then the fractional mass, m_{BH} , to a first extent, may be considered as independent of the vortex mass and bulge to vortex major semiaxis ratio.

The mere existence of a fundamental plane (Djorgovski and Davis, 1987; Dressler et al., 1987) indicates that structural properties in spheroids (elliptical galaxies and spiral bulges) span a narrow range, suggesting some self-regulating mechanism must be at work during formation and evolution. In particular, projected light profiles exhibit a large degree of homogeneity

and may well be fitted by the $r^{1/4}$ de Vaucouleurs law. Accordingly, a narrow range may safely be expected also for the factor, $1 - [(\sigma_{B0})_{33}/(\sigma_B)_{33}]^2$, appearing in Eq. (33), which makes the hole mass, M_H , depend only on the product, $R_B [(\sigma_B)_{33}]^2$, to a first extent.

If, in addition, the bulge density profile is close to an isothermal sphere, then the central velocity dispersion projected on the line of sight, σ_0 , is close to the rms velocity dispersion averaged on the mass, $(\sigma_B)_{33}$. Then the hole mass depends only on the product, $R_e \sigma_0^2$, to a first extent. Using the Faber-Jackson relation, $R_e \propto \sigma_0^2$, the standard M_H - σ_0 form ($M_H \propto \sigma_0^4$) is obtained (Escala, 2006).

A different analysis can be performed fixing the bulge mass, M_B , or the bulge to vortex mass ratio, m_{BV} , and considering the velocity ratio, $\eta = (\sigma_B)_{33}/\{[(v_V)_{qq}]^2 + [(\sigma_V)_{qq}]^2\}^{1/2}$, as a function of the bulge to vortex major axis ratio, y_{BV} . The related explicit expression is obtained by the combination of Eqs. (27), (28a), (28d), particularized to flat inner subsystems, which represents isofractional mass (i.e. fixed m_{BV} , m_{BH} , m_{VH}) curves in the $(Oy_{BV}\eta)$ plane.

The fractional masses, by definition, are related as $m_{BV} = m_{BH}/m_{VH}$, where $0 \leq m_{VH} \leq 5$ in the cases of interest. On the other hand, a correlation between bulge and hole mass, yielding $229 < m_{BH} < 795$, with a preferred value, $m_{BH} \approx 427$, has been deduced from recent observations (Marconi and Hunt, 2003). The assumption of constant m_{BH} implies isofractional mass curves in the $(Oy_{BV}\eta)$ plane depend on a single fractional mass, m_{VH} . Different cases in the range of interest, for $m_{BH} = 427$, are shown by full curves plotted in Fig. 1. Counterparts corresponding to an estimated upper ($m_{BH} = 229$) and lower ($m_{BH} = 795$) limit to the M_H - M_B relation (Marconi and Hunt, 2003), are shown by dashed and dotted curves, respectively. Different curves of each class (from top to bottom) correspond to $m_{VH} = 0, 1, 2, 3, 4, 5$, respectively. The reference configuration, $(m_{BH}, m_{VH}, y_{BV}) = (427, 5, 14)$, is represented by an asterisk.

An inspection of Fig. 1 discloses the following features.

- (i) All curves exhibit an extremum point of maximum. Lower m_{BH} and/or m_{VH} correspond to lower maximum coordinates, and vice versa.
- (ii) All curves are close, one with respect to the other, when they are rising, on the left of the maximum.
- (iii) All curves are parallel, one with respect to the other, when they are declining, on the right of the maximum.
- (iv) Curves related to different fractional masses, m_{BH} and m_{VH} , could be nearly coincident for a convenient choice of values. This is the case for

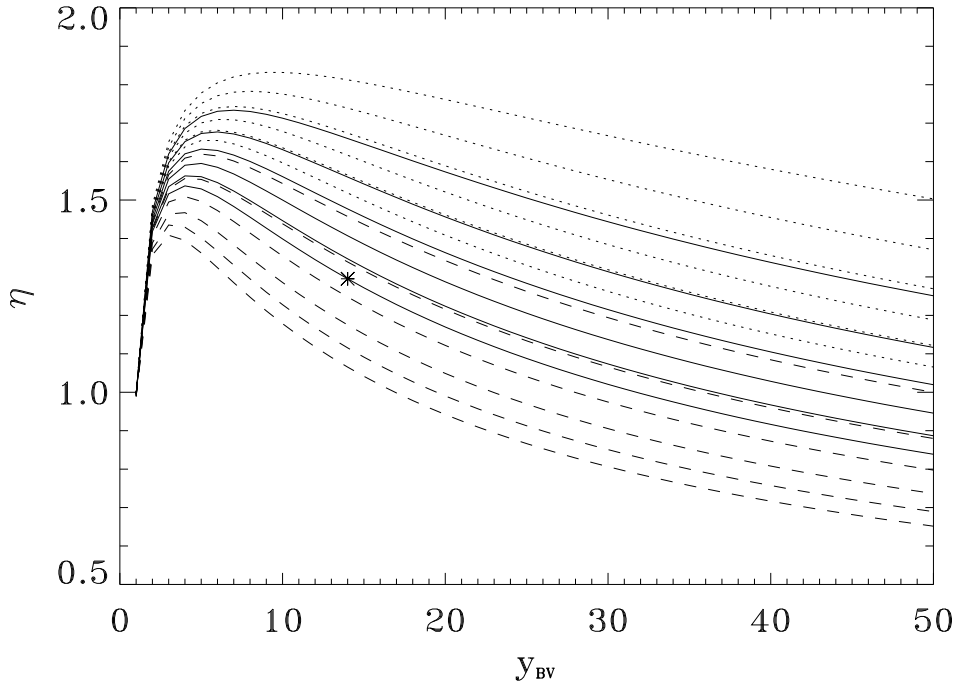


Figure 1: Isofractional mass curves in the $(Oy_{BV}\eta)$ plane for $m_{BH} = 427$ (full curves), which represents the preferred value of a recent interpolation of the empirical M_H-M_B relation (Marconi and Hunt, 2003). Counterparts corresponding to an estimated upper ($m_{BH} = 229$, dashed curves) and lower ($m_{BH} = 795$, dotted curves) limit to the M_H-M_B relation (Marconi and Hunt, 2003), are also shown. Different curves of each class (from top to bottom) correspond to $m_{VH} = 0, 1, 2, 3, 4, 5$, respectively. The reference configuration, $(m_{BH}, m_{VH}, y_{BV}) = (427, 200, 14)$, is represented by an asterisk.

$(m_{BH}, m_{VH}) = (427, 1)$ and $(795, 4)$, plotted in Fig. 1 as full and dotted lines, respectively.

3.4 Special cases

Aiming to see the model at work, two special cases shall be considered, where vortex rotation curves have been deduced from observations: NGC 4374 (M84) and NGC 4486 (M87). Parameter values of interest are listed in Tab. 1. Bulge data and related uncertainties are taken from a recent investigation (Cappellari et al., 2006), and errors are propagated using a standard quadratic formula. Vortex data are taken from different sources for NGC 4374 (Bower et al., 1998) and NGC 4486 (Macchetto et al., 1997).

NGC/M	4374/84		4486/87	
R_e/kpc	6.15 \mp 1.88	(1)	7.96 \mp 3.23	(1)
$\sigma_e/(\text{km s}^{-1})$	278 \mp 14	(1)	298 \mp 15	(1)
R'_V/pc	164 \mp 50	(2)	35 \mp 14	(3)
$V_V \sin i/(\text{km s}^{-1})$	250 \mp 150	(2)	500 \mp 100	(3)
i/deg	80 \mp 5	(2)	51 \mp 5	(3)
M_H/M_{10}	0.15 $^{+0.06}_{-0.11}$	(2)	0.32 \mp 0.09	(3)

Table 1: Parameter values related to NGC 4374 (M84) and NGC 4486 (M87). Captions: R_e - bulge effective (half-light) radius; σ_e - luminosity-weighted second moment of the line-of-sight velocity dispersion within the effective radius; R'_V - vortex radius at the end of the rotation velocity profile; V_V - vortex rotation velocity weighted on the mass, $M_V V_V^2 = \int_{S_V} \rho_V v_{\text{rot}}^2 dS_V$; i - inclination angle; M_H - hole mass; $M_{10} = 10^{10} m_\odot$. See text for details. The velocity conversion factors from [cm g s] to [kpc M_{10} Gyr] system of measure and vice versa are: $1 \text{ kpc Gyr}^{-1} = 0.978 461 942 118 946 6 \text{ km s}^{-1}$ and $1 \text{ km s}^{-1} = 1.022 012 156 992 443 \text{ kpc Gyr}^{-1}$, respectively. References: (1) Cappellari et al. (2006); (2) Bower et al. (1998); (3) Macchetto et al. (1997).

Rotation velocities weighted on the mass are roughly estimated as the mean of the maximum and the plateau value of the rotation curve, with no correction for inclination effects, whose contribution is thought to be negligible in the framework of the above approximation. The related uncertainty is assumed to be equal to the deviation from the mean. Radii correspond to the end of measured rotation curves. The related uncertainty is assumed to be equal (in percentage) to its bulge counterpart, $\sigma_{R'_V}/R'_V = \sigma_{R_B}/R_B$.

The virial equations, Eqs. (30a) and (30c), provide the remaining two unknowns: the fractional mass, m_{BH} , and the fractional radius, y_{BV} . The resulting position of NGC 4374 and NGC 4486 on the $(Oy_{\text{BV}}\eta)$ plane, is $(y_{\text{BV}}, \eta) = (37.5, 1.11)$ and $(113.68, 0.60)$, respectively. The dimensions of the error box can be evaluated by use of standard quadratic propagation formulae; the result is $(2\sigma_{y_{\text{BN}}}, 2\sigma_\eta) = (32.34, 1.44)$ and $(130, 0.30)$, respectively. The comparison with model predictions is shown in Figs. 2 and 3 for NGC 4374 and NGC 4486, respectively. The position of each galaxy at the centre of the error box is marked by an asterisk. The value of the fractional mass, m_{BH} , can be read near the corresponding curve on the right of the error box. The value of the fractional mass, m_{VH} , is null in all cases except lower full, dashed, and dotted curves, where $m_{\text{VH}} = 5$ and m_{BH} remains unchanged with respect to their upper counterparts (value labelled therein). The extreme cases still compatible with the error box, are represented by

dot-dashed curves. The centre of the error box is fitted by $m_{\text{BH}} = 230$ (NGC 4371) and $m_{\text{BH}} = 153$ (NGC 4486); the related curves are not plotted in Figs. 2 and 3, to avoid confusion.

3.5 Discussion

The application of the tensor virial theorem for subsystems to hole + vortex + bulge systems implies a number of restrictive assumptions to gain intrinsic simplicity related to analytical formulation. This is why the hole, the vortex, and the inner bulge are modelled as homogeneous, and the outer bulge as homeoidally striated. Accordingly, the bulge mass, M_{B} , the inner bulge mass, $M_{\text{I}} = M_{\text{B}}(R_{\text{V}})$, and the fractional radius, $y_{\text{BV}} = R_{\text{B}}/R_{\text{V}}$, are related by Eq. (24).

For assigned fractional masses, m_{BH} and m_{BV} , the velocity ratio, $\eta = (\sigma_{\text{B}})_{33} / \{[(v_{\text{V}})_{qq}]^2 + [(\sigma_{\text{V}})_{qq}]^2\}^{1/2}$, versus the fractional radius, $y_{\text{BV}} = R_{\text{B}}/R_{\text{V}}$, is represented by a selected curve on the $(\text{O}y_{\text{BV}}\eta)$ plane, as shown in Fig. 1. Interestingly, a fixed value of η below the maximum corresponds to two different configurations: a compact bulge on the left of the maximum, and an extended bulge on the right.

On the other hand, fixed m_{BV} and y_{BV} , imply larger m_{BH} passing from bottom to top along a vertical line, $y_{\text{BV}} = \text{const}$, as shown by the intersections of the above mentioned vertical line with the corresponding curves, see e.g., $y_{\text{BV}} = 50$ in Fig. 1. Accordingly, larger m_{BH} imply larger values of η and vice versa. Similar results hold for the fractional mass, m_{BV} , keeping m_{BH} fixed.

Upper curves of each series are related to massless vortexes, $m_{\text{VH}} = 0$. Test particles moving on circular and coplanar orbits, within a few hundred parsecs from the central hole, may be considered as massless vortexes. Then the knowledge of orbital parameters together with bulge effective radius and velocity dispersion, defines the position of the system on the $(\text{O}y_{\text{BV}}\eta)$ plane. The isofractional mass curve where the representative point lies, in turn, defines the value of the fractional mass, m_{BH} .

The application to NGC 4374 and NGC 4486, shown in Figs. 2 and 3, yields $8.5 < m_{\text{BH}} < 2250$ and $33 < m_{\text{BH}} < 400$, respectively. The empirical $M_{\text{B}} - M_{\text{H}}$ correlation (Marconi and Hunt, 2003), $229 < m_{\text{BH}} < 795$, lies within the uncertainty range for NGC 4374 but only partially for NGC 4486. The knowledge of the vortex density profile would provide a better determination of the mass-weighted rotation velocity, $(V_{\text{V}})_{qq}$, and then reduce the error box. In presence of a massive vortex ($m_{\text{VH}} = 5$), the hole mass has to be reduced by a factor 2-3 to get the fit.

The bulge mass can be estimated from Figs. 2 and 3, using hole mass values deduced from gas dynamics listed in Tab. 1. The result is: $M_{\text{B}}/M_{10} =$

$34.35_{-033.59}^{+550.65}$ and $48.96_{-041.37}^{+115.04}$ for NGC 4374 and NGC 4486, respectively.

On the other hand, the bulge mass may be inferred from the knowledge of the mass to luminosity ratio, the I -band magnitude, and the distance modulus (e.g., Caimmi and Valentinuzzi, 2008), using recent data and related uncertainties (Cappellari et al., 2006). The result is: $M_B/M_{10} = 72.70 \mp 67.50$ and 91.94 ∓ 80.92 for NGC 4374 and NGC 4486, respectively.

An alternative approach consists in dealing with the structural parameter estimate (Bender et al., 1992) of $M_B = (5/G)\sigma_o^2 R_e$, where σ_o is the bulge central velocity dispersion projected on the line of sight, and R_e is the bulge effective radius. An application to NGC 4374 can be found in an earlier attempt (Bower et al., 1998). Using recent data and related uncertainties (Cappellari et al., 2006) yields $M_B/M_{10} = 72.70 \mp 22.62$ and 108.12 ∓ 47.84 for NGC 4374 and NGC 4486, respectively. The uncertainty should be multiplied by ζ^\mp , if $5\zeta^- < 5 < 5\zeta^+$ is the scatter of the above relation.

Finally, the substitution of hole mass values listed in Tab.1 into the empirical M_B - M_H correlation, $229 < m_{BH} < 795$, with a preferred value, $m_{BH} = 427$, (Marconi and Hunt, 2003), yields $M_B/M_{10} = 64.05_{-043.44}^{+142.65}$ and $136.64_{-083.97}^{+189.31}$ for NGC 4374 and NGC 4486, respectively.

A comparison between the above results is shown in Fig. 4. Even if the current method is affected by a large upper uncertainty for NGC 4374, still it appears to be consistent with the other ones.

In general, a selected point on the $(Oy_{BV}\eta)$ plane is crossed by infinite curves of the kind plotted in Fig. 1, each characterized by a proper choice of fractional masses, (m_{BV}, m_{BH}) . In the limit of a massless vortex, $m_{BV} \rightarrow +\infty$, the model may be improved by replacing the inner bulge radius, $R_I = R_V$, with $R_I = R_H$. Accordingly, the bulge resembles a truncated isothermal sphere, where the central divergence of the density profile is avoided by the presence of a very small, homogeneous inner bulge.

The bulge velocity dispersion, $(\sigma_B)_{33}$, as a function of the bulge effective radius, R_e , in the limit of a massless vortex, is plotted in Fig. 5 for $R_I = R_V$ (full curves) and $R_I = R_H$ (dashed curves), related to: $(m_{BH}, R_V/\text{pc}) = (427, 125)$, $(230, 164)$, $(153, 70)$, in connection with Figs. 1, 2, 3, respectively. The position of the reference configuration (Fig. 1) is marked by an asterisk. The position of NGC 4374 and NGC 4486 and the related uncertainties, taken or deduced from recent observations (Cappellari et al., 2006), are marked by asterisks and rectangles, respectively. It can be seen that the assumption of a homogeneous inner bulge makes bulge velocity dispersion systematically decrease for fixed bulge effective radius, but the error is comparable with observational uncertainties.

The assumption of isotropic bulge stress tensor is acceptable for the special cases to which the model has been applied. More specifically, both NGC

4374 and NGC 4486 appear to be only slightly flattened. Even if the shape is entirely due to velocity dispersion, the stress tensor is expected to be moderately anisotropic provided the system is seen edge-on, and can be considered isotropic to a first extent. It is the case for NGC 4486, but not for NGC 4374 (Bender et al., 1992). If, on the other hand, the system is seen head-on, the line of sight coincides with the polar axis and what is deduced from observations is related to $(\sigma_B)_{33}$, regardless of the properties of the stress tensor. Strictly speaking, the degree of anisotropy and the inclination angle should be specified, in order to express the bulge velocity dispersion component along the polar axis, $(\sigma_B)_{33}$, in terms of the luminosity-weighted second moment of the line-of-sight velocity distribution within the bulge effective radius, R_e .

4 Conclusion

The tensor virial theorem for subsystems has been formulated for three-component systems and further effort has been devoted to a special case where the inner subsystems and the central region of the outer one are homogeneous, the last surrounded by an isothermal homeoid. The virial equations have explicitly been written under the additional restrictions: (i) similar and similarly placed inner subsystems, and (ii) spherical outer subsystem. An application has been made to hole + vortex + bulge systems, in the limit of flattened inner subsystems, which implies three virial equations in three unknowns.

Using the Faber-Jackson relation, $(R_B)_e \propto \sigma_0^2$, the standard M_H - σ_0 form ($M_H \propto \sigma_0^4$) has been deduced from qualitative considerations. The projected bulge velocity dispersion to projected vortex velocity ratio, $\eta = (\sigma_B)_{33} / \{[(v_V)_{qq}]^2 + [(\sigma_V)_{qq}]^2\}^{1/2}$, as a function of the fractional radius, $y_{BV} = R_B/R_V$, and the fractional masses, $m_{BH} = M_B/M_H$ and $m_{BV} = M_B/M_V$, has been studied in the range of interest, $0 \leq m_{VH} = M_V/M_H \leq 5$ (Escala, 2006) and $229 \leq m_{BH} \leq 795$ (Marconi and Hunt, 2003), consistent with observations.

The related curves have been shown to be similar to Maxwell velocity distributions, which implies a fixed value of η below the maximum corresponds to two different configurations: a compact bulge on the left of the maximum, and an extended bulge on the right. All curves have been seen to lie very close one to the other on the left of the maximum, and parallel one to the other on the right.

On the other hand, fixed m_{BH} or m_{BV} , and y_{BV} , have been found to imply more massive bulges passing from bottom to top along a vertical line on the $(Oy_{BV}\eta)$ plane, and vice versa. The model has been applied to NGC 4374

and NGC 4486, taking the fractional mass, m_{BH} , and the fractional radius, y_{BV} , as unknowns, and the bulge mass has been inferred and compared with results from different methods. In presence of a massive vortex ($m_{\text{VH}} = 5$), the fit has been provided by hole mass 2-3 times lower with respect to the case of a massless vortex. Finally, it has been shown that the assumptions of homogeneous inner bulge and isotropic stress tensor hold to an acceptable extent, at least in the special cases taken into consideration.

Acknowledgements

Thanks are due to S. Masiero for fruitful discussions.

References

- [1] Bender, R., Burstein, D., Faber, S.M., 1982. ApJ 399, 462.
- [2] Bilic, N., 2006. Arxiv: astro-ph/0610657v2.
- [3] Binney, J., Tremaine, S., 1987. *Galactic Dynamics*, Princeton University Press, New Haven.
- [4] Bower, G.A., Green, R.F., Danks, A., et al., 1988. ApJ 492, L111.
- [5] Brosche, P., Caimmi, R., Secco, L., 1983. A&A 125, 338.
- [6] Caimmi, R. 1991. ApSS 180, 211.
- [7] Caimmi, R. 1993. ApJ 419, 615.
- [8] Caimmi, R. 1995. ApJ 441, 533.
- [9] Caimmi, R., 2007. SerAJ 174, 13.
- [10] Caimmi, R., Secco, L., Brosche, P., 1984. A&A 139, 411.
- [11] Caimmi, R., Secco, L. 1992. ApJ 395, 119.
- [12] Caimmi, R., Secco, L., 2001. AN 322, 217.
- [13] Caimmi, R., Secco, L., 2002. AN 323, 13.
- [14] Caimmi, R., Marmo, C., 2003. NewA 8, 119.
- [15] Caimmi, R., Valentinuzzi, T. 2008. Arxiv:astro-ph/0801.3630.

- [16] Cappellari, M., Bacon, R., Bureau, M., et al., 2006. MNRAS 366, 1126.
- [17] Chandrasekhar, S. 1969. *Ellipsoidal Figures of Equilibrium*, Yale University Press, New Haven.
- [18] Djorgowski, S.G., Davis, M., 1987. ApJ 313, 59.
- [19] Downes, D., Solomon, P.M., 1998. ApJ 507, 615.
- [20] Dressler, A., Lynden-Bell, D., Burstein, D., et al., 1987. ApJ 313, 42.
- [21] Escala, A., 2006. ApJ 648, L13.
- [22] Ferrarese, L., Ford, H., 2005. Space Sci. Rev. 116, 523.
- [23] Gebhardt, K., Bender, F., Bower, G., et al., 2000. ApJ 539, L13.
- [24] King, A.R., Pringle, J.E., Hofmann, J.A., 2008. MNRAS 385, 1621.
- [25] Limber, D.N., 1959. ApJ 130, 414.
- [26] Macchetto, F., Marconi, A., Axon, D.J., et al., 1997. ApJ 489, 579.
- [27] MacMillan, D.W. 1930. *The Theory of the Potential*, Dover Publications, Inc. New York, 1958.
- [28] Maoz, E., 1998. ApJ 494, L181.
- [29] Marconi, A., Hunt, L.H., 2003. ApJ 589, L21.
- [30] Merritt, D., 2006. Rep. Prog. Phys. 69, 2513.
- [31] Miller, M.C., 2006. MNRAS 367, L32.
- [32] Neutsch, W., 1979. A&A 72, 339.
- [33] Roberts, P.H., 1962. ApJ 136, 1108.

Appendix

A Ellipsoid shape factors: special cases

Let a_1, a_2, a_3 , $a_1 \geq a_2 \geq a_3$, be semiaxes of a generic ellipsoid, and $\epsilon_{pq} = a_p/a_q$ related axis ratios. The shape factors, B_p and B_{pr} , defined by Eqs. (20b) and

	oblong	flat	prolate	oblate	spherical
ϵ_{21}	0	ϵ_f	ϵ_p	1	1
ϵ_{31}	0	0	ϵ_p	ϵ_o	1
B_1	$+\infty$	$\pi/2$	γ/ϵ_p^2	α/ϵ_o	2/3
B_2	1	$\pi/2$	α	α/ϵ_o	2/3
B_3	1	0	α	$\epsilon_o\gamma$	2/3
B_{11}	$+\infty$	$3\pi/8$	w_3/ϵ_p^2	w_1/ϵ_o	2/5
B_{12}	$+\infty$	$3\pi/8$	w_2/ϵ_p^4	w_1/ϵ_o	2/5
B_{13}	$+\infty$	$+\infty$	w_2/ϵ_p^4	w_2/ϵ_o	2/5
B_{21}	0	$3\pi/8$	w_2	w_1/ϵ_o	2/5
B_{22}	1/2	$3\pi/8$	w_1	w_1/ϵ_o	2/5
B_{23}	1/2	$+\infty$	w_1	w_2/ϵ_o	2/5
B_{31}	0	0	w_2	$\epsilon_o^3 w_2$	2/5
B_{32}	1/2	0	w_1	$\epsilon_o^3 w_2$	2/5
B_{33}	1/2	0	w_1	$\epsilon_o w_3$	2/5

Table 2: Values of ellipsoid shape factors, B_p and B_{pr} , related to limiting configurations defined by the values of the axis ratios, ϵ_{21} and ϵ_{31} . For oblong configurations, B_1 and B_{11} diverge as $\epsilon^2\gamma$, B_{12} and B_{13} as ϵ^2 . For flat configurations, B_{13} and B_{23} diverge as ϵ^{-1} .

(25g), respectively, in terms of their usual counterparts (e.g., Chandrasekhar, 1969, Chap. 3, §21; Caimmi, 1991, 1995), read:

$$B_p = \epsilon_{p2}\epsilon_{p3}A_p ; \quad (34)$$

$$B_{pr} = \epsilon_{p2}\epsilon_{p3}A_{pr}a_p^2 ; \quad (35)$$

$$\frac{B_{pr}}{B_p} = \frac{A_{pr}a_p^2}{A_p} ; \quad (36)$$

and a number of special cases are listed in Tab. 2 for limiting configurations.

The range of validity of the related independent variables, ϵ_f , ϵ_p , ϵ_o , and ϵ , is:

$$0 < \epsilon_f \leq 1 ; \quad 0 < \epsilon_p < 1 ; \quad 0 < \epsilon_o < 1 ; \quad (37a)$$

$$\epsilon = \epsilon_{31}, \quad 0 < \epsilon < 1, \quad \text{oblate} ; \quad (37b)$$

$$\epsilon = \epsilon_{21}^{-1} = \epsilon_{31}^{-1}, \quad 1 < \epsilon < +\infty, \quad \text{prolate} ; \quad (37c)$$

and the explicit expression of the functions, α , γ , w_1 , w_2 , w_3 , reads:

$$\alpha = \begin{cases} \frac{\epsilon}{1-\epsilon^2} \left[\frac{\arcsin \sqrt{1-\epsilon^2}}{\sqrt{1-\epsilon^2}} - \epsilon \right] ; & \text{oblate;} \\ \frac{\epsilon}{\epsilon^2-1} \left[\epsilon - \frac{\operatorname{arcsinh} \sqrt{\epsilon^2-1}}{\sqrt{\epsilon^2-1}} \right] ; & \text{prolate;} \end{cases} \quad (38)$$

$$\gamma = \begin{cases} \frac{2}{1-\epsilon^2} \left[1 - \epsilon \frac{\arcsin \sqrt{1-\epsilon^2}}{\sqrt{1-\epsilon^2}} \right] ; & \text{oblate;} \\ \frac{2}{\epsilon^2-1} \left[\epsilon \frac{\operatorname{arcsinh} \sqrt{\epsilon^2-1}}{\sqrt{\epsilon^2-1}} - 1 \right] ; & \text{prolate;} \end{cases} \quad (39)$$

$$w_1 = \frac{1}{4} (3\alpha - \epsilon^2 w_2) ; \quad w_2 = \frac{\gamma - \alpha}{1 - \epsilon^2} ; \quad w_3 = \frac{2}{3} (1 - \epsilon^2 w_2) ; \quad (40)$$

where, in addition (e.g., Caimmi, 1991):

$$2\alpha + \gamma = 2 ; \quad \lim_{\epsilon \rightarrow 1} \alpha = \lim_{\epsilon \rightarrow 1} \gamma = \frac{2}{3} ; \quad \lim_{\epsilon \rightarrow 0} \alpha = 0 ; \quad \lim_{\epsilon \rightarrow 0} \gamma = 2 ; \quad (41)$$

$$\lim_{\epsilon \rightarrow 0} \frac{\alpha}{\epsilon} = \frac{\pi}{2} ; \quad \lim_{\epsilon \rightarrow +\infty} \alpha = 1 ; \quad \lim_{\epsilon \rightarrow +\infty} \gamma = 0 ; \quad \lim_{\epsilon \rightarrow +\infty} \epsilon \gamma = 0 ; \quad (42)$$

$$\lim_{\epsilon \rightarrow +\infty} \epsilon^2 \gamma = +\infty ; \quad \lim_{\epsilon \rightarrow 1^-} w_2 = \lim_{\epsilon \rightarrow 1^+} w_2 = \frac{2}{5} . \quad (43)$$

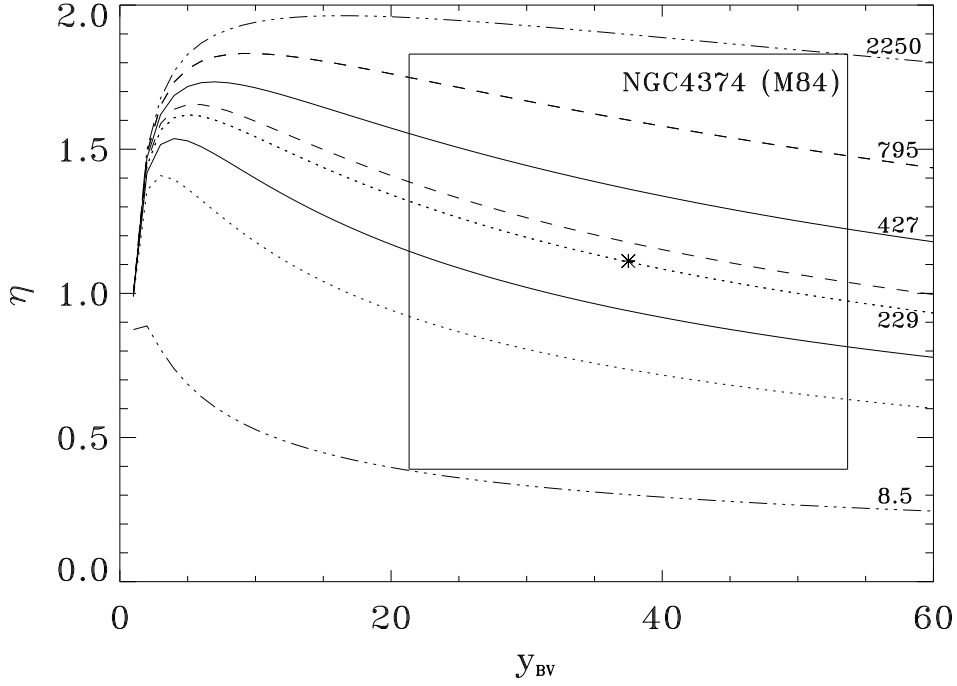


Figure 2: Comparison between model predictions and data from observations for NGC 4374 (M84). The position of the galaxy at the centre of the error box (deduced from values listed in Tab. 1) is marked by an asterisk. The value of the bulge to hole mass ratio, m_{BH} , can be read near the corresponding curve on the right of the box error. The value of the vortex to hole mass ratio, m_{VH} , is null in all cases except lower full, dashed, and dotted curves, where $m_{\text{VH}} = 5$ and m_{BH} remains unchanged with respect to their upper counterparts (value labelled therein). The extreme cases still compatible with the error box, are represented by dot-dashed curves. The centre of the error box is fitted by $m_{\text{BH}} = 230$ (not represented).

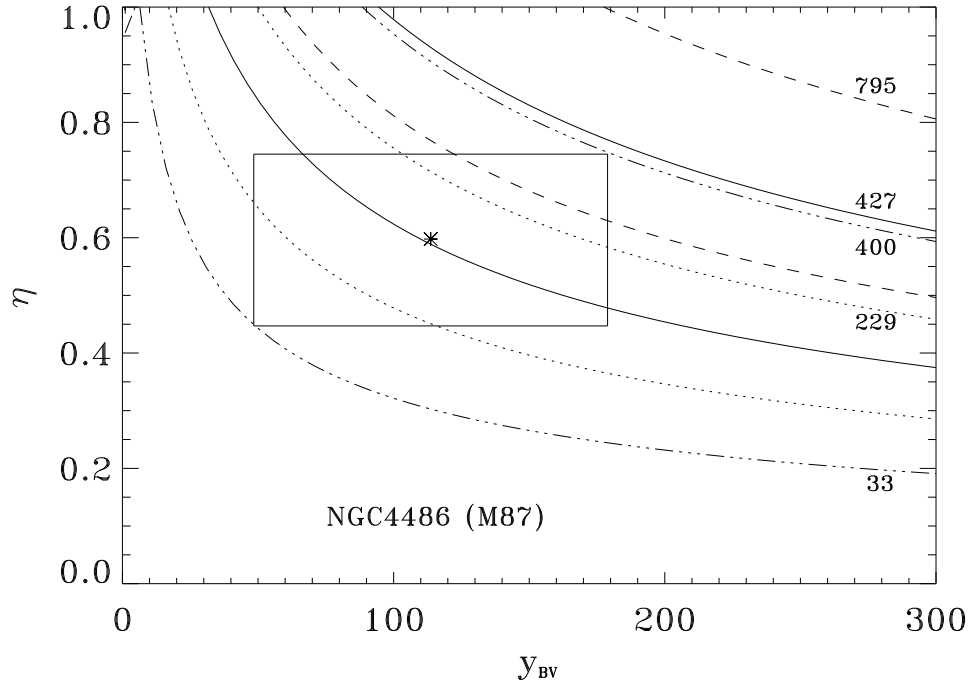


Figure 3: Comparison between model predictions and data from observations for NGC 4486 (M87). The position of the galaxy at the centre of the error box (deduced from values listed in Tab. 1) is marked by an asterisk. The value of the bulge to hole mass ratio, m_{BH} , can be read near the corresponding curve on the right of the box error. The value of the vortex to hole mass ratio, m_{VH} , is null in all cases except lower full, dashed, and dotted curves, where $m_{\text{VH}} = 5$ and m_{BH} remains unchanged with respect to their upper counterparts (value labelled therein). The extreme cases still compatible with the error box, are represented by dot-dashed curves. The centre of the error box is fitted by $m_{\text{BH}} = 153$ (not represented).

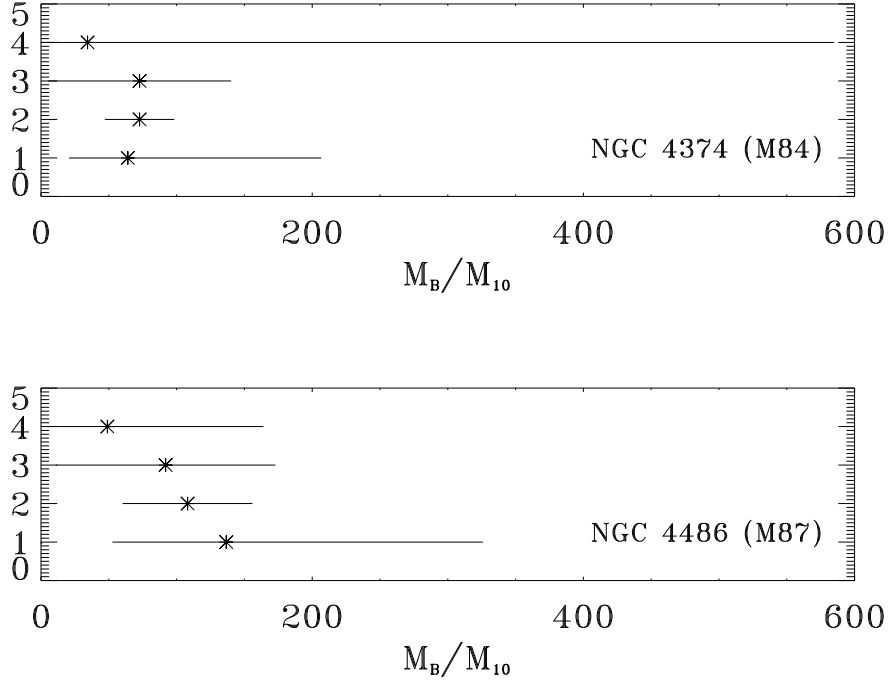


Figure 4: The bulge mass deduced from different methods, for NGC 4374 (M84, top) and NGC 4486 (M87, bottom). Different values in ordinate are deduced from: 1 - the empirical M_B - M_H correlation, $229 < m_{BH} < 795$, with a preferred value, $m_{BH} = 427$, (Marconi and Hunt, 2003), using hole mass values listed in Tab.1; 2 - the structural parameter estimate (Bender et al., 1992) of $M_B = (5/G)\sigma_o^2 R_e$, where σ_o is the bulge central velocity dispersion projected on the line of sight, and R_e is the bulge effective radius (the upper and lower limit should be multiplied by ζ^+ and ζ^- , respectively, where $5\zeta^- < 5 < 5\zeta^+$ is the scatter of the above relation); 3 - the knowledge of the mass to luminosity ratio, the I -band magnitude, and the distance modulus (e.g., Caimmi and Valentinuzzi, 2008), using recent data and related uncertainties (Cappellari et al., 2006); 4 - Figs.2 and 3, using hole mass values deduced from gas dynamics listed in Tab.1. Values of M_B/M_{10} for NGC 4374: 1 - $64.05_{+142.65}^{-043.44}$; 2 - 72.70 ∓ 22.62 ; 3 - 72.70 ∓ 67.50 ; 4 - $34.35_{+550.65}^{-033.59}$. Values of M_B/M_{10} for NGC 4486: 1 - $136.64_{+189.31}^{-083.97}$; 2 - 108.12 ∓ 47.84 ; 3 - 91.94 ∓ 80.92 ; 4 - $48.96_{+115.04}^{-041.37}$.

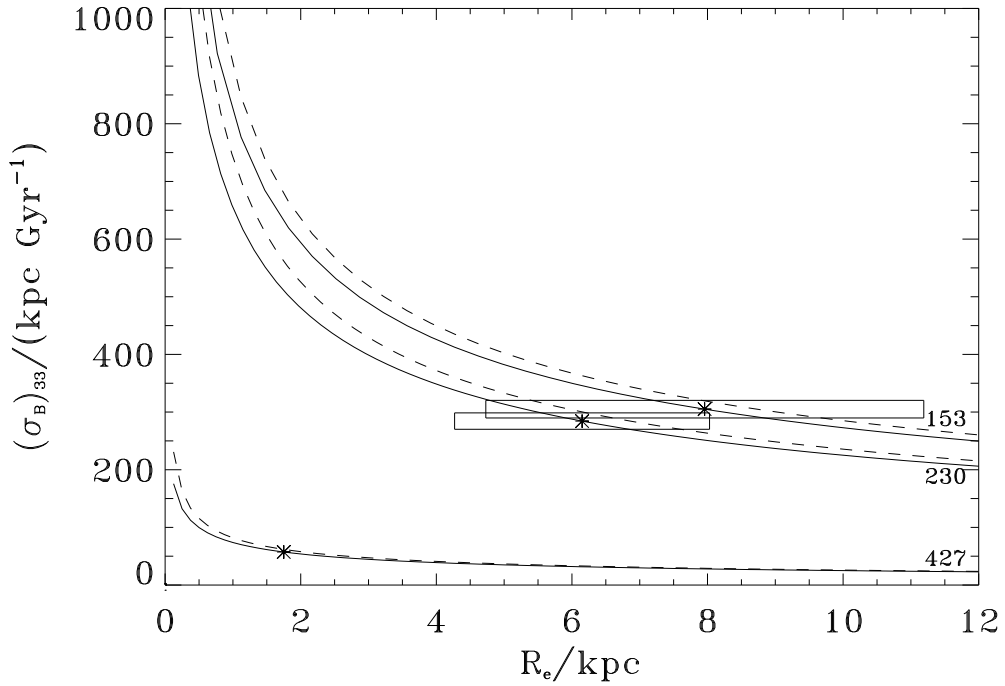


Figure 5: The bulge velocity dispersion, $(\sigma_B)_{33}$, as a function of the bulge effective radius, R_e , in the limit of a massless vortex, for $R_I = R_V$ (full curves) and $R_I = R_H$ (dashed curves), related to: $(m_{\text{BH}}, R_V/\text{pc}) = (427, 125)$, $(230, 164)$, $(153, 70)$, in connection with Figs. 1, 2, 3, respectively. The position of the reference configuration (Fig. 1) is marked by an asterisk. The position of NGC 4374 (Fig. 2) and NGC 4486 (Fig. 3) and the related uncertainties, taken or deduced from recent observations (Cappellari et al., 2006), are marked by asterisks and rectangles, respectively.